Modeling of Argon Gas Behavior in Continuous Casting of Steel

Hyunjin Yang, Surya P. Vanka and Brian G. Thomas

Abstract In continuous casting of steel, argon gas injection is a popular method to reduce nozzle clogging. Multiphase turbulent flow of molten steel with argon gas through complicated-geometry nozzles increases the complexity of the flow dynamics. In this study, these complex multiphase turbulent flow behaviors are simulated in a lab-scale continuous caster using a new hybrid model that involves a Eulerian-Eulerian (EE) model coupled simultaneously with a Discrete Phase Model (DPM). The complex behavior of the argon gas including formation of gas pockets, intermittent shearing off of the gas pockets, volumetric expansion, coalescence and breakup of bubbles, and transport of the bubbles in both the nozzle and mold are all simulated. The model is validated with measurements on a benchmark experiment of liquid-metal argon flow in a laboratory-scale system. This hybrid model is a promising tool to estimate realistic bubble size distributions and multiphase flow in a real caster.

Keywords Bubble size distribution · Coalescence · Breakup · Volumetric expansion · Shearing off

H. Yang (✉) · S. P. Vanka
Department of Mechanical Science and Engineering, University of Illinois at Urbana-Champaign, 1206 W. Green Street, Urbana, IL 61801, USA
e-mail: hyang69@illinois.edu

S. P. Vanka
e-mail: spvanka@illinois.edu

B. G. Thomas
Department of Mechanical Engineering, Colorado School of Mines, Brown Hall W370-B, 1610 Illinois Street, Golden, CO 80401, USA
e-mail: bgthomas@mines.edu

L. Nastac et al. (eds.), *CFD Modeling and Simulation in Materials Processing 2018*, The Minerals, Metals & Materials Series,
https://doi.org/10.1007/978-3-319-72059-3_12

Introduction

In continuous casting of steel, argon gas injection has an important influence on the fluid flow in the mold, including surface velocity, level fluctuations, and the consequent entrainment of mold slag and formation of other defects. The bubble size distribution is very important, controlling not only the flow pattern [1], but also the distribution of bubbles and particles entrapped into the solidifying shell [2]. This size distribution is very difficult to determine, and is an ongoing issue in computational modeling where unjustified assumptions must be made. A previous study [3] showed that the evolving argon bubble size distribution is a consequence of several phenomena: the formation of argon gas pockets in low-velocity regions inside the nozzle, intermittent shearing off of the gas pockets, bubble interactions such as coalescence and breakup, and volumetric expansion of the bubbles according to the surrounding liquid steel pressure. To accurately model the evolution of the bubble size distribution locally and transiently, sophisticated numerical and mathematical models are needed to simulate the complex argon gas behavior are necessary. In this work, a new hybrid model EEDPM is developed to model all of the phenomena mentioned above.

Model Description

Governing Equations of EEDPM

As the name of the model suggests, the governing equations are composed of two parts: an Eulerian-Eulerian (EE) model calculates velocity and volume fraction fields of each phase with a shared pressure field [4] from a continuity and Navier Stokes equations for each phase.

$$\frac{\partial(\alpha_k \rho_k)}{\partial t} + \nabla \cdot (\alpha_k \rho_k \boldsymbol{u}_k) = 0 \tag{1}$$

$$\frac{\partial(\alpha_k \rho_k \boldsymbol{u}_k)}{\partial t} + \nabla \cdot (\alpha_k \rho_k \boldsymbol{u}_k \boldsymbol{u}_k) = -\alpha_k \nabla p + \nabla \cdot \left(\mu_k \alpha_k \left(\nabla \boldsymbol{u}_k + \nabla \boldsymbol{u}_k^T\right)\right) + \alpha_k \rho_k \boldsymbol{g} + \boldsymbol{F_D} \tag{2}$$

A DPM model tracks each bubble as a point-mass, tracking position and velocity of the bubble [5].

$$\rho_g V_p \frac{d\boldsymbol{v_i}}{dt} = V_c(\boldsymbol{F_D} + \boldsymbol{F}_V + \boldsymbol{F}_P + \boldsymbol{F_B}) \tag{3}$$

$$\frac{d\boldsymbol{x_i}}{dt} = \boldsymbol{v_i} \tag{4}$$

These two models are run together as separate models in the same domain, but are coupled in several ways: the DPM momentum terms (RHS of Eq. 3) depend on the flow field from the EE model. Drag, virtual mass, pressure gradient and buoyancy forces are considered [6]. The DPM bubble size also evolves transiently by bubble interactions (coalescence and breakup), and volumetric expansion. At the same time, the instantaneous, spatially varying DPM bubble size distribution is given to the EE model, where it influences the drag force $\boldsymbol{F_D}$ between the gas and liquid phases in the EE model. Here, Tomiyama drag force model is used for the drag [7]. As the EE liquid phase flow field is changed by the drag force based on the DPM bubble size, this model system is two-way coupled. Consequently, this hybrid model can predict the spatially and time-varying bubble size distributions. Mass conservation problems are avoided because no mass is exchanged between the two models. For turbulence modeling, SST k-ω model is used with this EEDPM multiphase flow model. These governing equations are solved with ANSYS-Fluent using extensive user-defined subroutines developed specifically for this work.

Modeling of Shearing off Process

Figure 1 shows a flow chart of the overall algorithm of EEDPM including the shearing off process. To simulate the shearing off process of small bubbles from a large gas pocket, a new mathematical model is developed [8]. To locate the gas pockets, the model uses the gas volume fraction field from the EE model solution. The EE model captures both flow recirculation zones and gas pocket formation. To extract a sharp interface, α^*, from the continuous gas volume fraction field, α, a

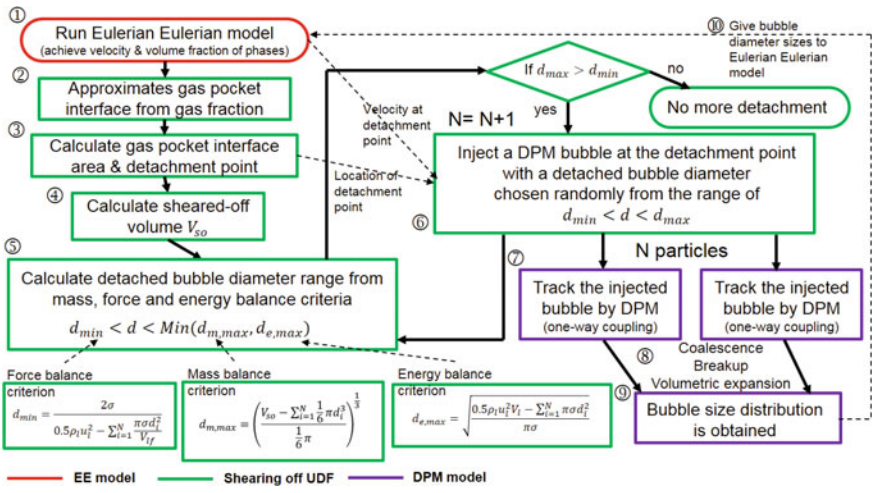

Fig. 1 Flow chart of EEDPM including shearing off process

criterion function is used ($\alpha^* = 1\ if\ \alpha \geq 0.95, otherwise\ \alpha^* = 0$). After approximating the gas pocket interface, the interface area (A_{int}) and detachment point of small bubbles are calculated numerically. The detachment point is assumed to be the lowest point of the gas pocket. The sheared off volume from the gas pocket is calculated by multiplying the interface area by the thickness of the sheared off layer ($V_{so} = A_{int}\delta_g^*$). The sheared off gas layer thickness (δ_g^*) is calculated using boundary layer theory. Once the sheared off volume is calculated, it is redistributed into small DPM bubbles. According to previous works for bubble breakup, the daughter bubble size is a stochastic variable [9]. Thus, the detached bubble size by the shearing off process is assumed to be a random variable (all sizes have equal probability). However, it is still important to specify a range of allowable daughter bubble sizes using mass, force and energy balance criteria. By adjusting the criteria of Luo and Svendsen (1996) [10] and Wang et al. [11], energy and force criteria are derived for the shearing off process (⑤ in Fig. 1). Also, a new mass criterion is added based on mass conservation, so that the total volume of detached bubbles cannot exceed the sheared off volume from the gas pocket. The force criterion generates the lower bound, and the mass and energy criteria generate the upper bound of bubble size range. The daughter bubbles must satisfy all three criteria. Then, the daughter bubble size is decided through a random generator in the range, and a bubble is injected at the detachment point as a Discrete Phase Model (DPM) bubble with that bubble size. The bounds evolve because mass, momentum and energy are consumed as bubbles detach from the gas pocket: the upper bound of bubble size decreases, and the lower bound increases. The shearing off process ends when the upper bound becomes less than the lower bound. The shearing off frequency is found by dividing the gas pocket length by the average liquid velocity. Detached DPM bubbles change their size transiently by coalescence, breakup and volumetric expansion. The locally and time-varying bubble size distribution obtained from DPM bubbles is updated every time step to EE model for the calculation of accurate local drag force.

Modeling of Bubble Interactions

Figure 2 shows a flow chart of the coalescence model. First, collision is easily handled from the calculation of distance between a pair of DPM bubbles. Here, only distances of pairs located in the same computational cell are considered to decrease the computational cost from n^2 to n. If the distance between a pair is smaller than a sum of radius of two bubbles ($r_1 + r_2$), the pair is counted as a collided pair. And then, the coalescence efficiency e is calculated based on the drainage model [12], based on the drainage time ($t_{drainage}$) and the contact time ($t_{contact}$), from previous models [13]. Here, we assume constant e = 0.1. Coalescence is randomly determined with the probability based on the coalescence efficiency after collision. If two bubbles coalesce, a coalesced bubble size and a velocity of the bubble are

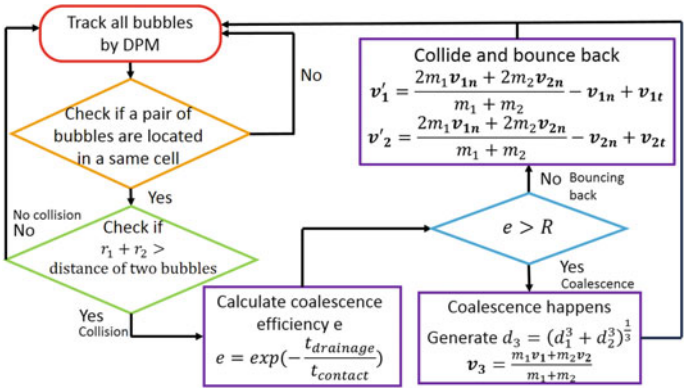

Fig. 2 Flow chart of coalescence model

calculated by mass and momentum conservation. Otherwise, two bubbles bounce apart via an elastic collision. This is a reasonable assumption for small bubbles since the strong surface tension makes them act like hard spheres. Figure 3 describes the algorithm of the breakup model for DPM bubbles. The first criterion of breakup is to check the bubble size: if the size is greater than the maximum stable bubble size d_{crit} [14], the first criterion is satisfied. And then, a range of smaller daughter bubble size is calculated by mass and force balance criteria. If the upper bound is greater than the lower bound, the model counts that the bubble breaks up and a smaller daughter bubble diameter is randomly determined in the range. The other daughter bubble size is automatically determined by the mass conservation.

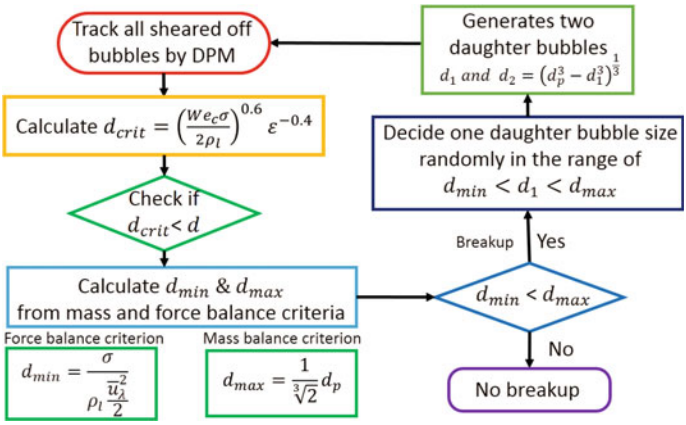

Fig. 3 Flow chart of breakup model

Modeling of Volumetric Expansion

Gas bubbles can expand or shrink according to the surrounding liquid pressure field. To calculate the size change of bubble due to the liquid pressure, a cubic equation with respect to r_{new} (new bubble radius) is derived from the Young-Laplace equation and the ideal gas law [6]:

$$p_{l,new}\left(\frac{d_{new}}{2}\right)^3 + 2\sigma\left(\frac{d_{new}}{2}\right)^2 - p_{g,old}\left(\frac{d_{old}}{2}\right)^3 = 0 \tag{5}$$

By solving this equation for each DPM bubble, volumetric expansion or shrinkage of bubbles by the surrounding liquid pressure is calculated. In this work, the volumetric expansion is counted every 10-time step to decrease the computational cost.

Results and Discussion

An experiment of lab-scale stopper rod system done by Timmel's research group [3] is benchmarked to validate the EEDPM hybrid model. As shown in Fig. 4, this is a slot-shaped geometry: front view geometry is projected into thickness direction by 12 mm. Liquid Galinstan is supplied from the top of funnel shape and flows

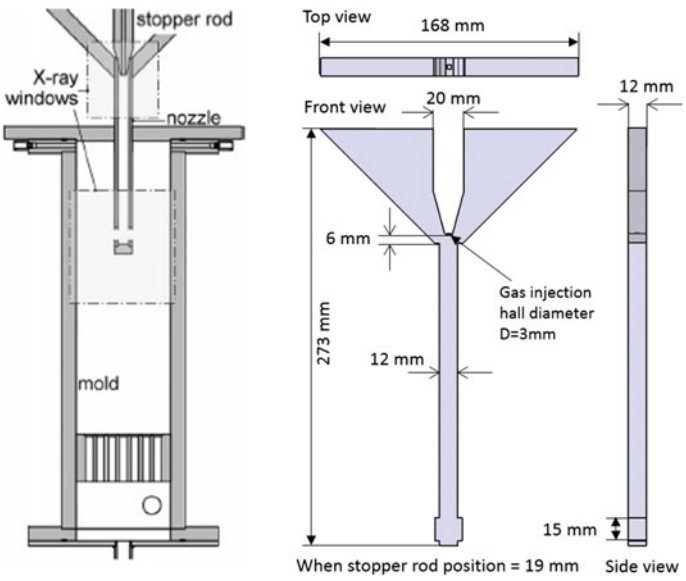

Fig. 4 Geometry of lab-scale stopper rod system

Table 1 Operating condition and material properties [3]

Operating condition	Value	Material property	Value
Operating temperature	293 K	Galinstan density	6440 kg/s
Stopper rod position	19 mm	Galinstan viscosity	0.0024 Pa
Tundish level	70 mm	Galinstan surface tension coefficient	0.718 N/m
Galinstan flow rate	140 cm/s	Argon gas density	1.6228 kg/m^3
Argon gas flow rate	0.24 cm/s	Argon gas viscosity	2.125 $\times$ 10^{-5} Pas
Submergence depth	92 mm		
Wall roughness	Smooth wall (acrylic)		
Mold size	100 $\times$ 15 $\times$ 426 mm^3		

downward by gravity. Argon gas is injected from the tip of stopper rod. Operating conditions and material properties are given in Table 1.

Due to the low melting point of Galinstan, this experiment is conducted at room temperature. Argon gas behavior is measured through X-ray shots from front: projected gas volume fraction field is obtained from the X-ray intensity (brightness $\cong$ volume fraction). Since this geometry is much smaller, thinner, and rectangular than the real scale stopper-rod system, the argon gas behavior may be different than a commercial casting nozzle. However, this experiment is still valuable for validation as: (1) bubbles behavior in liquid metal is measured (with similar high surface tension and buoyancy), (2) experiments of bubbly downflow with sudden expansion are rare.

Figure 5 shows the gas pocket formation at the recirculation zones through accumulation of argon gas from the stopper tip and the detachment of small bubbles from them. The shearing off model injects DPM bubbles as detached small bubbles. The transient solution shows that large bubbles ($d > 6$ mm) are detached intermittently, but break down to smaller bubbles in few time steps due to the development of high turbulence dissipation rate near the gas pockets.

Figure 6 displays the sheared DPM bubbles with flow field information. Due to the very thin mold, jets injecting from the nozzle ports obstruct most of the bubbles from rising to the top once bubbles flow into the lower mold. It is observed that bubbles circulate in the lower roll and experience coalescence and breakup repeatedly. Very large bubbles ($d > 7$ mm) evolve due to serial coalescence and are

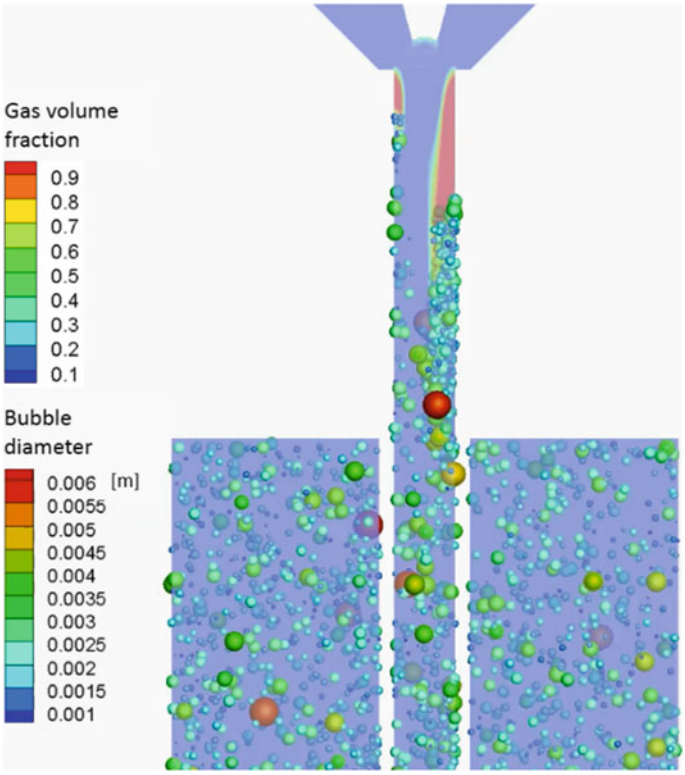

Fig. 5 Sheared off DPM bubbles from gas pockets at t = 22.0925 s

able to overcome the jet obstruction and float to the top sporadically. Figure 7 shows the DPM bubbles with the turbulence dissipation rate field. High ε is observed near the bottom of the port due to the development of swirl and it causes breakup of big bubbles (d > 6 mm) when they pass through the port. Also, two relatively-large bubbles are observed staying at the top of each port due to the coalescence of accumulated DPM bubbles at the recirculation zones.

Figure 8 describes the time-averaged results of number, size and residence time of DPM bubbles in the domain. In the nozzle, roughly 1000 bubbles are found and zone 1 has the largest number of bubbles due to the accumulation of bubbles in the recirculation zones near the inlet of nozzle. Residence time of zone 1 is longer than zone 2 because of the same reason. The average bubble size increases as it goes down except zone 4 due to the residence time effect: big bubbles try to stay longer in the nozzle due to stronger buoyancy. The reason that zone 4 does not follow this

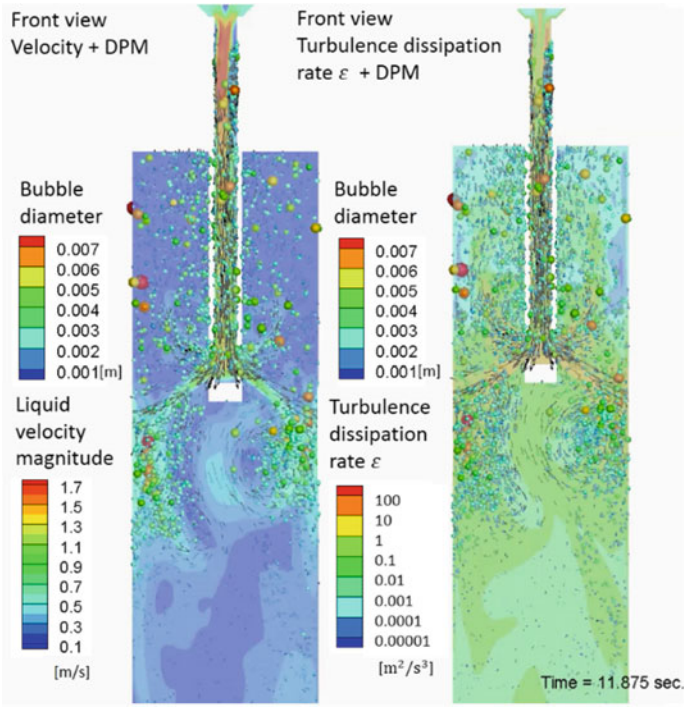

Fig. 6 DPM bubble distribution with velocity (left) and turbulence dissipation rate field (right) at t = 11.875 s

trend is because of the breakup of bubbles by the swirl developed at the bottom of the nozzle. In case of the bubbles in the mold, 4000 bubbles are observed in total, and zone 7 has the largest number of bubbles due to the jet obstruction effect. A decrease of average bubble size between zone 4 (in nozzle) and 7 (in mold) is caused by the swirl effect discussed in Fig. 7. Also, zone 7 has the largest average bubble size in the mold because of the coalescence of bubbles: high number density of bubbles results more collision, and ultimately more chance of coalescence. The residence time of zone 7 and 8 is longer than other zones, due to the jet obstruction effect.

Figure 9 shows the transition of bubble size distribution by time. It shows that the bubble size distribution does not change much by time. Figure 10 compares the bubble size distribution with the experimental measurement [3]. The calculation results show reasonable agreement. The majority of bubbles have d = 1–3 mm because the average turbulence dissipation rate in the nozzle ($\varepsilon = 1-10\,\mathrm{m}^2/\mathrm{s}^3$) allows maximum stable bubble sizes in the range.

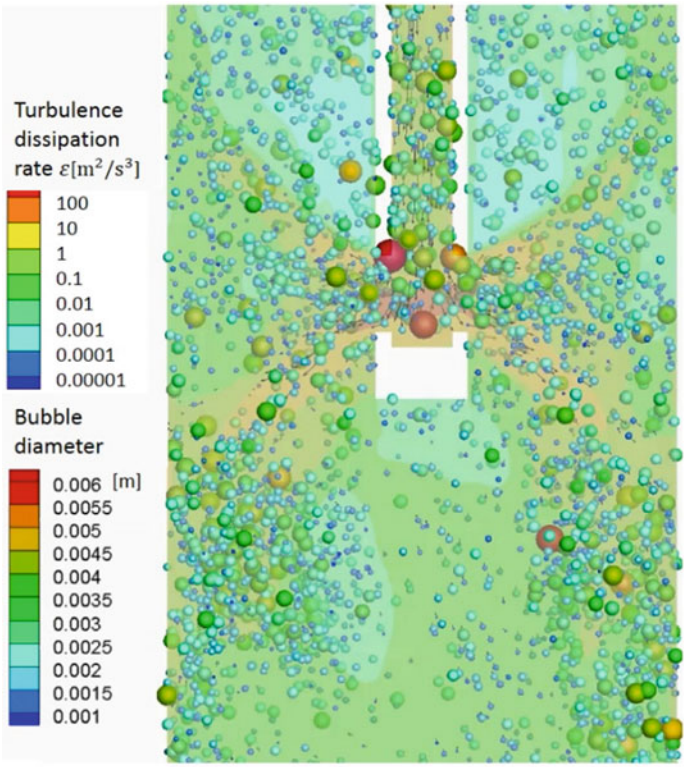

Fig. 7 DPM bubble distribution with turbulence dissipation rate field near the bottom of the nozzle at t = 22.23 s

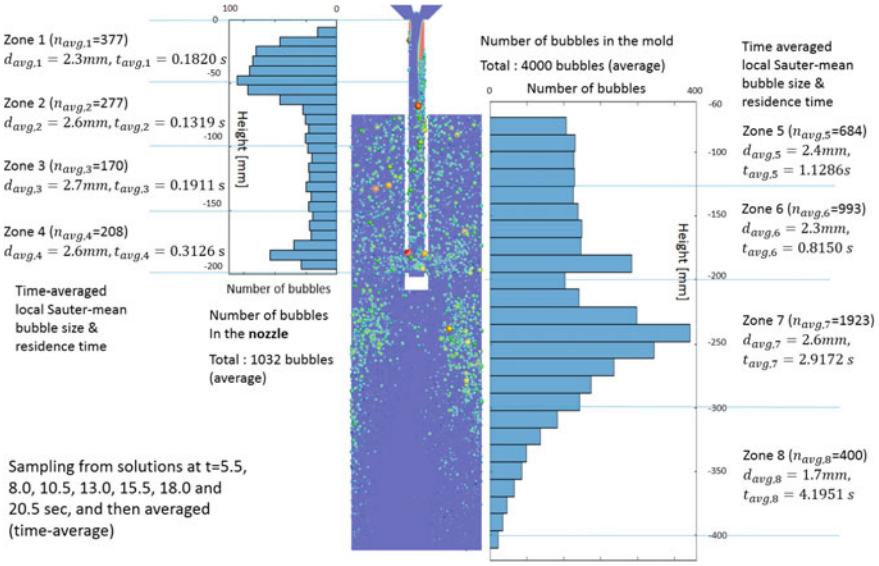

Fig. 8 Number, size and residence time of DPM bubbles in the domain

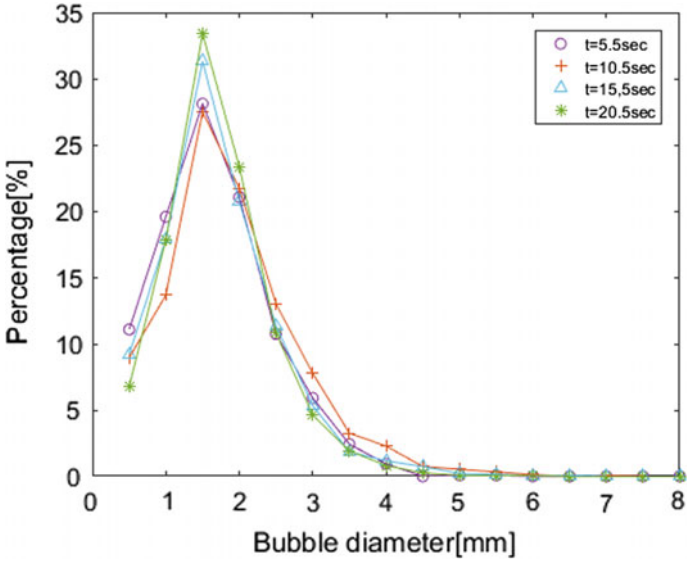

Fig. 9 Transition of bubble size distribution by time

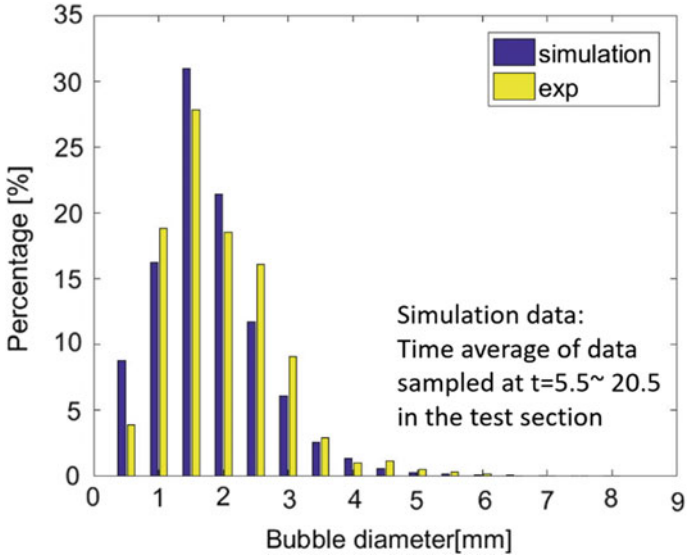

Fig. 10 Comparison of bubble size distribution to the measurement

Conclusions

The lab-scale stopper rod system is simulated through the new hybrid model EEDPM. The complex behavior of argon gas in the process is modeled, including formation of argon gas pockets, intermittent shearing off of the gas pockets, volumetric expansion, coalescence and breakup of bubbles. Those models are validated by comparison with the measured bubble size distribution in the mold. This model is able to simulate realistic phenomena observed in the experiment such as intermittent floatation of big bubbles near the narrow face in the lower mold by the serial coalescence, and breakup of big bubbles at the bottom of the nozzle port by the swirl development. The turbulent dissipation rate strongly affects the bubble size distribution through the maximum stable bubble size in the breakup model. The majority of bubbles have d = $1 \sim 3$ mm corresponding to the average turbulence dissipation rate $\varepsilon = 1 \sim 10 \mathrm{m}^2/s^3$ in the nozzle flow. Due to the balance of all of the phenomena changing the bubble size, the bubble size distribution does not change much by time.

Acknowledgements This work was supported by the National Science Foundation (Grant No. CMMI 15-63553) and the Continuous Casting Consortium, University of Illinois at Urbana-Champaign, USA.

Nomenclature

Symbols

A_{int} Interface area of gas pocket, d: diameter of a bubble, $\boldsymbol{F}$: force, $\boldsymbol{g}$: gravity

m_b Mass of a bubble, N: total number of bubble created by shearing off p: pressure

R Random number between 0 and 1, r: bubble radius, t: time, $\boldsymbol{u}$: velocity field, u: velocity magnitude, $\bar{u}_\lambda$: eddy velocity, V: volume, $\boldsymbol{v_i}$: velocity of ith DPM bubble, $\boldsymbol{v_i'}$: velocity of i-th DPM bubble after collision

We_c Critical Weber number, $\boldsymbol{x_i}$: ith DPM bubble velocity, α: EE volume fraction field

α^* Approximated volume fraction field, μ: viscosity, ρ: density, ε: liquid turbulence dissipation rate

σ Surface tension coefficient, δ_g^*: sheared off gas layer thickness

$\sum_{j=1}^{N}$ Summation of sheared off bubbles created in one shearing off process

Subscripts

k and q	Arbitrary phase (gas or liquid), B: buoyancy, D: drag, g: gas, l: liquid, lf: liquid film
N	Normal, t: tangent, new: new position, old: old position, P: pressure gradient, p: parent bubble
SO	Sheared off, V: virtual mass, 1: smaller bubble in a pair, 2: larger bubble in a pair
3	Created bubble by coalescence

References

1. Liu Z, Qi F, Li B, Jiang M (2014) Multiple size group modeling of polydispersed bubbly flow in the mold: an analysis of turbulence and interfacial force models. Metall Mater Trans B 46:933–952
2. Jin K, Thomas BG, Ruan X (2015) Modeling and measurements of multiphase flow and bubble entrapment in steel continuous casting. Metall Mater Trans B 47:548–565
3. Timmel K, Shevchenko N, Röder M, Anderhuber M, Gardin P, Eckert S, Gerbeth G (2014) Visualization of liquid metal two-phase flows in a physical model of the continuous casting process of steel. Metall Mater Trans B 46:700–710
4. Harlow FH, Amsden AA (1975) Numerical calculation of multiphase fluid flow. J Comput Phys 17:19–52
5. Riley JJ (1974) Diffusion experiments with numerically integrated isotropic turbulence. Phys Fluids 17(2): 292–297
6. Yang H, Vanka SP, Thomas BG (2017) Hybrid eulerian eulerian discrete phase model of turbulent bubbly flow. In: Proceedings of the ASME 2017 international mechanical engineering congress & exposition, ASME. Tampa, Florida
7. Tomiyama A, Kataoka I, Zun I, Sakaguchi T (1998) Drag coefficients of single bubbles under normal and micro gravity conditions. JSME Int J Ser B 41:472–479
8. Yang H, Thomas BG (2017) Multiphase flow and bubble size distribution in continuous casters using a hybrid EEDPM model. STEELSIM 2017, Quingdao, China
9. Hesketh RP, Etchells AW, Russell TWF (1991) Experimental observations of bubble breakage in turbulent flow. Ind Eng Chem Res 30:835–841
10. Luo H, Svendsen HF (1996) Theoretical model for drop and bubble breakup in turbulent dispersions. AIChE J 42:1225–1233
11. Wang T, Wang J, Jin Y (2003) A novel theoretical breakup kernel function for bubbles/droplets in a turbulent flow. Chem Eng Sci 58:4629–4637
12. Prince MJ, Blanch HW (1990) Bubble coalescence and break-up in air-sparged bubble columns. AIChE J 36:1485–1499
13. Liao Y, Lucas D (2009) A literature review of theoretical models for drop and bubble breakup in turbulent dispersions. Chem Eng Sci 64:3389–3406
14. Evans GM, Jameson GJ, Atkinson BW (1992) Prediction of the bubble size generated by a plunging liquid jet bubble column. Chem Eng Sci 47:3265–3272